# Coherent and incoherent dynamics in excitonic energy transfer: correlated fluctuations and off-resonance effects

Dara P. S. McCutcheon[1, 2, *] and Ahsan Nazir[1, †]

[1] *Department of Physics and Astronomy, University College London, Gower Street, London WC1E 6BT, United Kingdom*
[2] *London Centre for Nanotechnology, University College London*

(Dated: September 22, 2010)

We study the nature of the energy transfer process within a pair of coupled two-level systems (donor and acceptor) subject to interactions with the surrounding environment. Going beyond a standard weak-coupling approach, we derive a master equation within the polaron representation that allows for investigation of both weak and strong system-bath couplings, as well as reliable interpolation between these two limits. With this theory, we are then able to explore both coherent and incoherent regimes of energy transfer within the donor-acceptor pair. We elucidate how the degree of correlation in the donor and acceptor fluctuations, the donor-acceptor energy mismatch, and the range of the environment frequency distribution impact upon the energy transfer dynamics. In the resonant case (no energy mismatch) we describe in detail how a crossover from coherent to incoherent transfer dynamics occurs with increasing temperature [Phys. Rev. Lett. **103**, 146404 (2009)], and we also explore how fluctuation correlations are able to protect coherence in the energy transfer process. We show that a strict crossover criterion is harder to define when off-resonance, though we find qualitatively similar population dynamics to the resonant case with increasing temperature, while the amplitude of coherent population oscillations also becomes suppressed with growing site energy mismatch.

## I. INTRODUCTION

A fascinating series of recent experiments demonstrating signatures of quantum coherence in the energy transfer dynamics of a variety of systems[1–9] has sparked renewed interest in modeling excitation energy transfer beyond standard methods.[10–19] This process, which occurs when energy absorbed at one site (the donor) is transferred to another nearby site (the acceptor) via a virtual photon,[20] is often considered to be incoherent; the result of weak donor-acceptor interactions, treated perturbatively using Fermi's golden rule.[21,22] However, though this approach has proved to be immensely successful when applied in many situations,[23,24] accounting for *quantum coherence* within the energy transfer dynamics requires an analysis beyond straightforward perturbation theory in the donor-acceptor interaction.

An alternative starting point for investigations into coherent energy transfer is to treat the system-environment interaction as a perturbation instead. Such weak-coupling theories, often referred to as being of Redfield or Lindblad type depending upon the approximations made in their derivation,[25] have been successfully applied to elucidate a number of effects that could be at play in multi-site donor-acceptor complexes. Examples include studying the interplay of coherent dynamics and dephasing in promoting efficient energy transfer in quantum aggregates,[26–32] exploring the role of environmental correlations in tuning the energy transfer process,[33] and extensions to assess the potential importance of non-Markovian effects.[34,35]

Nevertheless, in order to properly understand the transition from coherent to incoherent energy transfer which occurs as the system-environment coupling or temperature is increased,[11,36–38] it is necessary to be able to describe the system dynamics beyond either of these limiting cases.[24,39,40] Building on earlier work,[36,41–43] a number of methods have been put forward to accomplish this. For example, modifications to both Redfield[44–47] and Förster[48–50] theory have extended the range of validity of both approaches. Moreover, it is possible to define a new perturbation term through the small polaron transformation,[51] which under certain conditions allows interpolation between the Redfield and Förster limits.[11–13] For particular forms of system-environment interaction, this can also be achieved through the hierarchical equations of motion technique.[16,52] Numerically exact calculations, based, for example, on path integral,[15,53] numerical renormalisation group[54] and density matrix renormalisation group[14] methods, have also been applied to study energy transfer beyond perturbative approaches.

In this work, we investigate the conditions under which coherent or incoherent motion is expected to dominate the energy transfer dynamics of a model donor-acceptor pair. Following Ref. 11, we employ a Markovian master equation derived within the polaron representation for this purpose, since it allows for a consistent analysis of the dynamics from weak to strong system-bath coupling (or, equivalently, low to high temperatures).[51,55] In addition to presenting a full derivation of the theory, we also extend it to explore in detail the important effects of donor-acceptor energy mismatch, deriving analytical forms for the dissipative dynamics valid over a large range of parameter space. Furthermore, we move beyond the scaling limit studied in Ref. 11 to consider an environment frequency distribution of finite extent, characterised by a high-frequency cut-off in the bath spectral density. In the resonant case (no energy mis-

match) we define a strict crossover temperature above which the energy transfer dynamics ceases to be coherent.[11] Of particular practical interest is the role played by correlations between the donor and acceptor environmental fluctuations, suggested as a mechanism by which quantum coherence may survive in the energy transfer process under otherwise adverse conditions.[1,4,9,11,53,56–60] These correlations are also easily treated within our formalism, through position-dependent couplings between the system and the common environment. As the donor and acceptor are brought closer together, there comes a point at which their separation becomes comparable to, or smaller than, the wavelength of relevant modes in the bath. As this happens, fluctuations at each site become ever more correlated, and dephasing effects are suppressed. We shall show, consequently, that as the level of correlation increases, so too does the crossover temperature to the incoherent regime. Hence, strong correlations lead to the survival of coherence at high temperatures.

Off-resonance, we find that it is less straightforward to define a crossover temperature. In contrast to the resonant case, for sufficient energy mismatch between the donor and acceptor, increasing the temperature causes the amplitude of the coherent contribution to decrease, though not to disappear altogether. In principle, it then becomes possible for a coherent component to exist in the dynamics at all but infinite temperatures. Although we are then unable to define a crossover in quite the same way, we still find that bath correlations have a qualitatively similar effect to the resonant case, protecting coherence in the transfer process.

The paper is organised as follows. In Section II we introduce our model, and derive a master equation describing the donor-acceptor dynamics within the polaron representation. Section III considers the resonant case and the coherent-incoherent crossover. In Section IV we investigate off-resonant energy transfer and obtain analytic expressions for the dynamics in a number of limits. Finally, in Section V we summarise our results.

## II. POLARON TRANSFORM MASTER EQUATION

### A. The system and polaron transformation

We consider a donor-acceptor pair ($j = 1, 2$), each site of which is modeled as a two-level system with ground state $|G\rangle_j$, excited state $|X\rangle_j$, and energy splitting $\epsilon_j$. The pair interact via Coulombic energy transfer with strength $V$, which is responsible for the transfer of excitation from one site to the other. The environment surrounding the donor-acceptor pair is modelled as a common bath of harmonic oscillators, coupled linearly to the excited state of each site. The total system-bath Hamiltonian is therefore written (where $\hbar = 1$)

$$\begin{aligned} H &= \sum_{j=1}^{2} \epsilon_j |X\rangle_j\langle X| + V(|XG\rangle\langle GX| + |GX\rangle\langle XG|) \\ &\quad + \sum_{j=1}^{2} |X\rangle_j\langle X| \sum_{\mathbf{k}} (g_{\mathbf{k}}^{(j)} b_{\mathbf{k}}^\dagger + g_{\mathbf{k}}^{(j)*} b_{\mathbf{k}}) + \sum_{\mathbf{k}} \omega_{\mathbf{k}} b_{\mathbf{k}}^\dagger b_{\mathbf{k}}, \end{aligned} \tag{1}$$

where the bath is described by creation (annihilation) operators $b_{\mathbf{k}}^\dagger$ ($b_{\mathbf{k}}$) with corresponding angular frequency $\omega_{\mathbf{k}}$, and wavevector $\mathbf{k}$. The system-bath couplings are given by $g_{\mathbf{k}}^{(j)}$. As in Ref. 11, we shall consider the case in which each site is coupled to the bosonic bath with the same magnitude $|g_{\mathbf{k}}|$, but make the separation between the sites explicit through position-dependent phases in the coupling constants of the form $g_{\mathbf{k}}^{(j)} = |g_{\mathbf{k}}| e^{i\mathbf{k}\cdot\mathbf{r}_j}$, with $\mathbf{r}_j$ being the position of site $j$. As we shall see, this form of coupling gives rise to correlations between the bath influences experienced at each site, allowing the range of totally correlated, partially correlated, and completely uncorrelated fluctuations to be explored.[11,53]

Inspection of Eq. (1) reveals that it generates dynamics in three decoupled subspaces, spanned by $\{|GG\rangle, \{|GX\rangle, |XG\rangle\}, |XX\rangle\}$. We are interested here in excitation energy transfer and therefore focus on the single-excitation subspace, $\{|GX\rangle, |XG\rangle\}$, in which this occurs. Relabelling $|XG\rangle \to |0\rangle$ and $|GX\rangle \to |1\rangle$, the Hamiltonian of the single-excitation subspace may be written

$$\begin{aligned} H_{\rm SUB} &= \epsilon_1 |0\rangle\langle 0| + \epsilon_2 |1\rangle\langle 1| + V(|0\rangle\langle 1| + |1\rangle\langle 0|) \\ &\quad + |0\rangle\langle 0| B_z^{(1)} + |1\rangle\langle 1| B_z^{(2)} + \sum_{\mathbf{k}} \omega_{\mathbf{k}} b_{\mathbf{k}}^\dagger b_{\mathbf{k}}, \end{aligned} \tag{2}$$

where we have defined the bath operators $B_z^{(j)} = \sum_{\mathbf{k}} (g_{\mathbf{k}}^{(j)} b_{\mathbf{k}}^\dagger + g_{\mathbf{k}}^{(j)*} b_{\mathbf{k}})$. A standard weak-coupling approach to the system dynamics would now be to derive a master equation for the evolution of the reduced system density operator under the assumption that the system-bath interaction terms, as written in Eq. (2), can be treated as weak perturbations.[25,61] In this work, we shall instead derive a master equation describing the donor-acceptor energy transfer dynamics in the polaron representation,[11–13,43,51,55] whereby we displace the bath oscillators depending on the system state. We may then identify alternative perturbation terms, which can be small over a much larger range of parameter space than those in the original representation. In particular, the polaron framework allows us to reliably explore from weak (single-phonon) to strong (multiphonon) coupling regimes between the system and the bath, provided that the energy transfer interaction $V$ does not become the largest energy scale in the problem (in which case the full polaron displacement is no longer appropriate[74]),

and that there is no infra-red divergence in its bath-renormalised value $V_R$ (see Eq. (8) below).[62] In contrast, with a weak system-bath coupling treatment we would only be able to probe single-phonon bath-induced processes, and hence not be able to properly explore the crossover from coherent to incoherent dynamics in which we are primarily interested.

To proceed, we thus apply a unitary transformation which displaces the bath oscillators according to the location of the excitation. Defining $H_P = \mathrm{e}^{S} H_{\rm SUB} \mathrm{e}^{-S}$, where

$$S = |0\rangle\langle 0|\, P(g_{\mathbf{k}}^{(1)}/\omega_{\mathbf{k}}) + |1\rangle\langle 1|\, P(g_{\mathbf{k}}^{(2)}/\omega_{\mathbf{k}}), \tag{3}$$

with bath operators $P(\alpha_{\mathbf{k}}) = \sum_{\mathbf{k}} (\alpha_{\mathbf{k}} b_{\mathbf{k}}^{\dagger} - \alpha_{\mathbf{k}}^{*} b_{\mathbf{k}})$, results in the polaron transformed spin-boson Hamiltonian[51] $H_P = H_0 + H_I$, with

$$H_0 = \frac{\epsilon}{2}\sigma_z + V_R \sigma_x + \sum_{\mathbf{k}} \omega_{\mathbf{k}} b_{\mathbf{k}}^{\dagger} b_{\mathbf{k}}, \tag{4}$$

and

$$H_I = V(B_x \sigma_x + B_y \sigma_y). \tag{5}$$

Here, the bias $\epsilon = \epsilon_1 - \epsilon_2$, gives the energy difference between the donor and acceptor, while the Pauli operators are defined in a basis in which $\sigma_z = |0\rangle\langle 0| - |1\rangle\langle 1| = |XG\rangle\langle XG| - |GX\rangle\langle GX|$. The bath operators appearing in Eq. (4) are constructed as $B_x = (1/2)(B_+ + B_- - 2B)$ and $B_y = (i/2)(B_+ - B_-)$, where

$$B_{\pm} = \prod_{\mathbf{k}} D\left( \pm \frac{(g_{\mathbf{k}}^{(1)} - g_{\mathbf{k}}^{(2)})}{\omega_{\mathbf{k}}} \right), \tag{6}$$

with displacement operators $D(\pm\alpha_{\mathbf{k}}) = \exp[\pm(\alpha_{\mathbf{k}} b_{\mathbf{k}}^{\dagger} - \alpha_{\mathbf{k}}^{*} b_{\mathbf{k}})]$. Note that the interaction terms in Eq. (5) therefore depend upon the difference in donor and acceptor system-bath couplings $g_{\mathbf{k}}^{(1)}$ and $g_{\mathbf{k}}^{(2)}$, respectively. Importantly, the term driving coherent energy transfer in Eq. (4) will not be treated perturbatively, but it does now have a bath-renormalised strength, $V_R = BV$, where

$$B = \exp\left[ -\sum_{\mathbf{k}} \frac{|g_{\mathbf{k}}|^2}{\omega_{\mathbf{k}}^2} (1 - \cos(\mathbf{k}\cdot\mathbf{d})) \coth(\beta\omega_{\mathbf{k}}/2) \right] \tag{7}$$

is the expectation value of the bath operators with respect to the free Hamiltonian: $B = \langle B_{\pm} \rangle_{H_0}$. The donor-acceptor separation is given by $\mathbf{d} = \mathbf{r}_1 - \mathbf{r}_2$.

In order to calculate the renormalisation factor, we take the continuum limit to convert the summation in Eq. (7) into an integral. Defining the bath spectral density $J(\omega) = \sum_{\mathbf{k}} |g_{\mathbf{k}}|^2 \delta(\omega - \omega_{\mathbf{k}})$, which contains information regarding both the density of oscillators in the bath with a given frequency, and also how strongly those oscillators interact with the donor-acceptor pair, and assuming a linear, isotropic dispersion relation, we find

$$B = \exp\left[ -\int_0^{\infty} \frac{J(\omega)}{\omega^2} (1 - F_D(\omega, d)) \coth(\beta\omega/2) \right]. \tag{8}$$

Here, $\beta = 1/k_B T$, while the function $F_D(\omega, d)$ captures the degree of spatial correlation in the bath fluctuations seen at each site, and is dependent upon the dimensionality of the system-bath interaction ($D = 1, 2, 3$).[33,53,63] In one dimension $F_1(\omega, d) = \cos(\omega d/c)$, with $c$ the bosonic excitation speed, in two dimensions $F_2(\omega, d) = J_0(\omega d/c)$, where $J_0(x)$ is a Bessel function of the first kind, and in three dimensions $F_3(\omega, d) = \mathrm{sinc}(\omega d/c)$. In all cases $F_D(\omega, d) \to 1$ as $d \to 0$, i.e. when the donor and acceptor are at the same position, bath fluctuations are perfectly correlated, and the energy transfer strength is not renormalised ($V_R \to V$). In fact, in this limit dissipative process are entirely suppressed (provided $|g_{\mathbf{k}}^{(1)}| = |g_{\mathbf{k}}^{(2)}|$) and energy transfer remains coherent for all times and in all parameter regimes in our model (the single-excitation subspace is then decoherence-free.[64,65]) In two and three dimensions, as $d \to \infty$, $F_D(\omega, d) \to 0$, and the renormalisation takes on the value that would be obtained by considering separate, completely uncorrelated baths surrounding the donor and acceptor. In the following, we shall characterise the degree of correlation in terms of the dimensionless parameter $\mu = c/d\omega_0$, where $\omega_0$ is a typical bath frequency scale (see Eq. (32) below). We therefore have $\mu = 0$ in the absence of correlations, $\mu < 1$ for weak correlations, and $\mu > 1$ for strong correlations.

### B. Markovian master equation

Having identified a new perturbation term by transforming our Hamiltonian to the polaron representation, we can now construct a master equation describing the evolution of the donor-acceptor pair reduced density operator $\rho$ up to second order in $H_I$. We employ a standard Born-Markov approach, which yields a polaron frame, interaction picture master equation of the form[25]

$$\frac{\partial \tilde{\rho}(t)}{\partial t} = -\int_0^{\infty} d\tau\, \mathrm{tr}_B\big[ [\tilde{H}_I(t), [\tilde{H}_I(t-\tau), \tilde{\rho}(t) \otimes \rho_B] \big], \tag{9}$$

where tildes indicate operators in the interaction picture, $\tilde{O}(t) = \mathrm{e}^{iH_0 t} O \mathrm{e}^{-iH_0 t}$, and $\mathrm{tr}_B$ denotes a trace over the bath degrees of freedom. In deriving Eq. (9) we have assumed: (i) factorising initial conditions for the joint system-bath density operator within the polaron frame, $\chi(0) = \rho(0) \otimes \rho_B$, with $\rho_B = e^{-\beta H_B}/\mathrm{tr}_B(e^{-\beta H_B})$ being a thermal equilibrium state of the bath; (ii) that by construction the interaction is weak in the polaron frame so that we may factorise the joint density operator as $\tilde{\chi}(t) = \tilde{\rho}(t)\rho_B$ at all times; (iii) that the timescale on which the donor-acceptor system evolves appreciably in both the Schrödinger and interaction pictures is large compared to the bath memory time $\tau_B$. Since, for the spectral density we shall consider below, $\tau_B \sim 1/\omega_c$, where $\omega_c$ is a high-frequency cutoff (see Eq. (32)), this is not too restrictive, as we must keep $V < \omega_c$ anyway in order for the polaron theory to work well. We note that interesting non-Markovian and non-equilibrium

bath effects have been explored in the polaron formalism in Refs. 12 and 13.

Inserting Eq. (5) into Eq. (9), and moving back into the Schrödinger picture, we arrive at our Markovian master equation describing the energy transfer dynamics within the single-excitation subspace, and written in the polaron frame as

$$\begin{aligned}\frac{\partial\rho(t)}{\partial t} =& -i[(\epsilon/2)\sigma_z + V_R\sigma_x, \rho(t)] \\ &- V^2\int_0^\infty \mathrm{d}\tau\Big([\sigma_x, \tilde{\sigma}_x(-\tau)\rho(t)]\Lambda_{xx}(\tau) \\ &\qquad + [\sigma_y, \tilde{\sigma}_y(-\tau)\rho(t)]\Lambda_{yy}(\tau) + \text{H.c.}\Big),\end{aligned} \tag{10}$$

where H.c. denotes Hermitian conjugation. The effect of the bath is now contained within the correlation functions $\Lambda_{ll}(\tau) = \langle B_l(\tau)B_l(0)\rangle_{H_0}$, which are given explicitly by

$$\Lambda_{xx}(\tau) = (B^2/2)(\mathrm{e}^{\phi(\tau)} + \mathrm{e}^{-\phi(\tau)} - 2), \tag{11}$$

$$\Lambda_{yy}(\tau) = (B^2/2)(\mathrm{e}^{\phi(\tau)} - \mathrm{e}^{-\phi(\tau)}), \tag{12}$$

where

$$\begin{aligned}\phi(\tau) = 2\int_0^\infty d\omega\Bigg[&\frac{J(\omega)}{\omega^2}(1 - F_D(\omega, d)) \\ &\times(\cos\omega\tau\coth(\beta\omega/2) - i\sin\omega\tau)\Bigg].\end{aligned} \tag{13}$$

Notice that the phonon propagator, $\phi(\tau)$, is correlation-dependent due to the factor $(1 - F_D(\omega, d))$, and so clearly the dissipative effect of the bath will be dependent upon the degree of correlation too. For example, as $d \to 0$, $F_D(\omega, d) \to 1$, and the dissipative contribution to Eq. (10) vanishes, as anticipated earlier.

### C. Evolution of the Bloch vector

We solve our master equation in terms of the Bloch vector, defined as $\boldsymbol{\alpha} = (\alpha_x, \alpha_y, \alpha_z)^T = (\langle\sigma_x\rangle, \langle\sigma_y\rangle, \langle\sigma_z\rangle)^T$. As we are working exclusively in the single-excitation subspace, $\alpha_x$ and $\alpha_y$ describe the coherences between the states $|0\rangle \equiv |XG\rangle$ and $|1\rangle \equiv |GX\rangle$, while $\alpha_z$ captures the donor-acceptor population transfer dynamics generated by the coupling $V$.

Though Eq. (10) is written in the Schödinger picture, it is still in the polaron frame, and so we must determine how expectation values in the polaron frame are related to those in the original, or "lab" frame. We can see this by writing $\dot{\alpha}_i = \mathrm{tr}_{S+B}(\sigma_i\dot{\chi}_L(t)) = \mathrm{tr}_{S+B}(\sigma_i\mathrm{e}^{-S}\dot{\chi}(t)\mathrm{e}^{S}) = \mathrm{tr}_{S+B}(\mathrm{e}^{S}\sigma_i e^{-S}\dot{\rho}(t)\rho_B)$, where $\chi_L(t) = e^{-S}\chi(t)e^{S}$ is the lab frame total density operator, and we have made use of the Born approximation in the polaron frame to write $\chi(t) = \rho(t)\rho_B$. Since $\mathrm{e}^{S}\sigma_x\mathrm{e}^{-S} = |1\rangle\langle 0|\,B_+ + |0\rangle\langle 1|\,B_-$, $\mathrm{e}^{S}\sigma_y\mathrm{e}^{-S} = i(|1\rangle\langle 0|\,B_+ - |0\rangle\langle 1|\,B_-)$, and $\mathrm{e}^{S}\sigma_z\mathrm{e}^{-S} = \sigma_z$, this implies that the lab Bloch vector elements are $\dot{\alpha}_i = B\dot{\alpha}_{iP}$, for $i = x, y$, and $\dot{\alpha}_z = \dot{\alpha}_{zP}$, where $\alpha_{iP}$ is an expectation value in the polaron frame: $\dot{\alpha}_{iP} = \mathrm{Tr}_S(\sigma_i\dot{\rho}(t))$. Alternatively, we can define a matrix $L$ which maps the polaron frame Bloch vector ($\boldsymbol{\alpha}_P$) to its lab frame counterpart ($\boldsymbol{\alpha}$): $\boldsymbol{\alpha} = L\cdot\boldsymbol{\alpha}_P$, where $L = \mathrm{diag}(B, B, 1)$.

Working in terms of the Bloch vector, we arrive at an equation of motion of the form

$$\dot{\boldsymbol{\alpha}}(t) = M\cdot\boldsymbol{\alpha}(t) + \boldsymbol{b}. \tag{14}$$

In the following, we shall often be interested in determining whether the energy transfer dynamics is predominantly coherent or incoherent. It is then helpful to write Eq. (14) as

$$\dot{\boldsymbol{\alpha}}'(t) = M\cdot\boldsymbol{\alpha}(t)', \tag{15}$$

with $\boldsymbol{\alpha}'(t) = \boldsymbol{\alpha}(t) - \boldsymbol{\alpha}(\infty)$, where $\boldsymbol{\alpha}(\infty) = -M^{-1}\cdot\boldsymbol{b}$ is the steady state. This makes clear that the nature of the energy transfer process lies solely in the matrix $M$, while the inhomogeneous term $\boldsymbol{b}$ is needed only in determining the steady state.

Equipped with the eigensystem of $M$, we may determine the corresponding time evolution as follows: an eigenvector of $M$, say $\boldsymbol{m}_i$, has equation of motion $\dot{\boldsymbol{m}}_i = q_i\boldsymbol{m}_i$, where $q_i$ is the corresponding eigenvalue. Its subsequent evolution then has the simple exponential form $\boldsymbol{m}_i(t) = \boldsymbol{m}_i\mathrm{e}^{q_i t}$. More generally, we can say that any initial state $\boldsymbol{\alpha}'(0)$ will have subsequent evolution

$$\boldsymbol{\alpha}'(t) = \sum_{i=1}^{3} a_i\boldsymbol{m}_i\mathrm{e}^{q_i t}, \tag{16}$$

where the coefficients $a_i$ are determined by the initial conditions (i.e. the solutions of $\boldsymbol{\alpha}'(0) = \sum_i a_i\boldsymbol{m}_i$). The solution to the full inhomogeneous equation is then found simply by addition of the steady state: $\boldsymbol{\alpha}(t) = \boldsymbol{\alpha}'(t) + \boldsymbol{\alpha}(\infty)$.

## III. RESONANT ENERGY TRANSFER

We start by considering the important special case of resonant energy transfer, in which the interplay of coherent and incoherent effects is particularly pronounced. As we shall see, in this situation it is relatively straightforward to derive a strict criterion governing when we expect the energy transfer dynamics to be able to display signatures of coherence.[11,51] Hence, resonant conditions provide a natural situation in which to begin to understand, for example, the role of bath spatial correlations[9,11,33,53,56–60] or the range of the bath frequency distribution in determining the nature of the energy transfer process.

Setting the donor-acceptor energy mismatch to zero, $\epsilon = 0$, we find from Eq. (10) dynamics generated by an

expression of the form $\dot{\boldsymbol{\alpha}} = M_R \cdot \boldsymbol{\alpha} + \boldsymbol{b}_R$, with

$$M_R = \begin{pmatrix} -(\Gamma_z - \Gamma_y) & 0 & 0 \\ 0 & -\Gamma_y & -2BV_R \\ 0 & B^{-1}(2V_R + \lambda_3) & -\Gamma_z \end{pmatrix}, \tag{17}$$

and $\boldsymbol{b}_R = (-B\kappa_x, 0, 0)^T$, where

$$\Gamma_y = 2V^2\gamma_{xx}(0), \tag{18}$$
$$\Gamma_z = V^2(\gamma_{yy}(2V_R) + \gamma_{yy}(-2V_R)) + 2V^2\gamma_{xx}(0), \tag{19}$$
$$\lambda_3 = 2V^2(S_{yy}(2V_R) - S_{yy}(-2V_R)), \tag{20}$$
$$\kappa_x = V^2(\gamma_{yy}(2V_R) - \gamma_{yy}(-2V_R)). \tag{21}$$

The rates and energy shifts are related to the response functions

$$K_{ii}(\omega) = \int_0^\infty d\tau \mathrm{e}^{i\omega\tau}\Lambda_{ii}(\tau) = \frac{1}{2}\gamma_{ii}(\omega) + iS_{ii}(\omega), \tag{22}$$

such that

$$\gamma_{ii}(\omega) = 2\mathrm{Re}[K_{ii}(\omega)] = \int_{-\infty}^{+\infty} d\tau \mathrm{e}^{i\omega\tau}\Lambda_{ii}(\tau), \tag{23}$$

and $S_{ii}(\omega) = \mathrm{Im}[K_{ii}(\omega)]$.

The resonant steady-state is straightforwardly found to be

$$\alpha_x(\infty) = -B\tanh(\beta V_R), \tag{24}$$

while $\alpha_y(\infty) = \alpha_z(\infty) = 0$. Notice that while this is of the same form as the steady-state that would be obtained from a weak system-bath coupling treatment,[25,66] $\alpha_x(\infty)$ is determined here by $V_R$, rather than the original coupling $V$, and there is also an extra factor of $B$ suppressing its magnitude.

The procedure described in Section II C to determine the time evolution of $\boldsymbol{\alpha}$ is somewhat unnecessary here, since the equation of motion for $\alpha_x$ is decoupled from that for $\alpha_y$ and $\alpha_z$. However, with some foresight we calculate the eigenvectors of $M_R$ in any case, finding

$$\boldsymbol{m}_1 = \Big\{1, 0, 0\Big\}^T, \tag{25}$$
$$\boldsymbol{m}_2 = \boldsymbol{m}_3^* = \Big\{0, \frac{B(\Gamma_z - \Gamma_y - i\xi_R)}{2(2V_R + \lambda_3)}, 1\Big\}^T, \tag{26}$$

with corresponding eigenvalues $q_1 = \Gamma_y - \Gamma_z$, and $q_2 = q_3^* = -(1/2)(\Gamma_y + \Gamma_z + i\xi_R)$. Thus, referring to Eq. (16), we see that

$$\xi_R = \sqrt{8V_R(2V_R + \lambda_3) - (\Gamma_z - \Gamma_y)^2} \tag{27}$$

determines whether any coherence exists within the energy transfer dynamics. Considering the initial state $\boldsymbol{\alpha}(0) = (0, 0, 1)^T$, corresponding to excitation of the donor, $\rho(0) = |0\rangle\langle 0| = |XG\rangle\langle XG|$, we find analytical

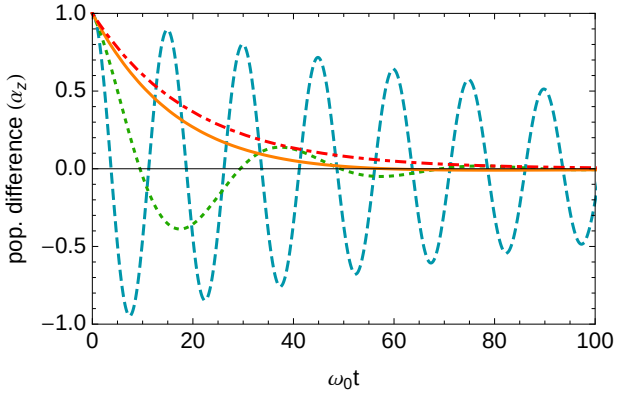


FIG. 1: Population difference as a function of scaled time $\omega_0 t$ for temperatures of $k_BT/\omega_0 = 1$ (blue dashed curve), $k_BT/\omega_0 = 5$ (green dotted curve), $k_BT/\omega_0 = 12$ (orange solid curve) and $k_BT/\omega_0 = 20$ (red dot-dashed curve). Parameters: $\alpha = 0.05$, $V/\omega_0 = 0.5$, $\omega_c/\omega_0 = 4$, $\epsilon = 0$ and $\mu = c/d\omega_0 = 0.5$.

forms for the evolution of the Bloch vector components:

$$\alpha_x(t) = -B\tanh(\beta V_R)(1 - \mathrm{e}^{-(\Gamma_y - \Gamma_z)t}), \tag{28}$$
$$\alpha_y(t) = -\frac{2BV_R}{\xi_R}\mathrm{e}^{-(\Gamma_y + \Gamma_z)t/2}\sin\Big(\frac{\xi_R t}{2}\Big), \tag{29}$$
$$\alpha_z(t) = \mathrm{e}^{-(\Gamma_y + \Gamma_z)t/2}\Big[\cos\Big(\frac{\xi_R t}{2}\Big) + \frac{\Gamma_y - \Gamma_z}{\xi_R}\sin\Big(\frac{\xi_R t}{2}\Big)\Big]. \tag{30}$$

Inspection of Eqs. (27) and (30) allows us to identify a crossover from coherent to incoherent motion in the energy transfer dynamics as the point at which oscillations in the population difference vanish:[11]

$$(\Gamma_z - \Gamma_y)^2 = 8V_R(2V_R + \lambda_3). \tag{31}$$

For $(\Gamma_z - \Gamma_y)^2 < 8V_R(2V_R + \lambda_3)$, $\xi_R$ is real and both the population difference and coherence $\alpha_y$ describe damped oscillations, while for $(\Gamma_z - \Gamma_y)^2 \geq 8V_R(2V_R + \lambda_3)$, $\xi_R$ is either zero or imaginary, with the resulting dynamics then being entirely incoherent.

To further analyse the behaviour of $\alpha_z(t)$, and the conditions for which the boundary defined by Eq. (31) is crossed, we now take a specific form for the system-bath spectral density. For a large enough bath we may approximate $J(\omega) = \sum_{\mathbf{k}} |g_{\mathbf{k}}|^2 \delta(\omega_{\mathbf{k}} - \omega)$ as a smooth function of $\omega$. In this work we consider a spectral density of the form

$$J(\omega) = \alpha\frac{\omega^3}{\omega_0^2}\mathrm{e}^{-\omega/\omega_c}, \tag{32}$$

where $\alpha$ is a dimensionless quantity capturing the strength of the system-bath interaction, and $\omega_0$ is a typical frequency of bosons in the bath, which sets an overall energy scale. The cubic frequency dependence in Eq. (32) is typical, for example, in describing dephasing in quantum dots due to coupling to acoustic phonons,[67] but can

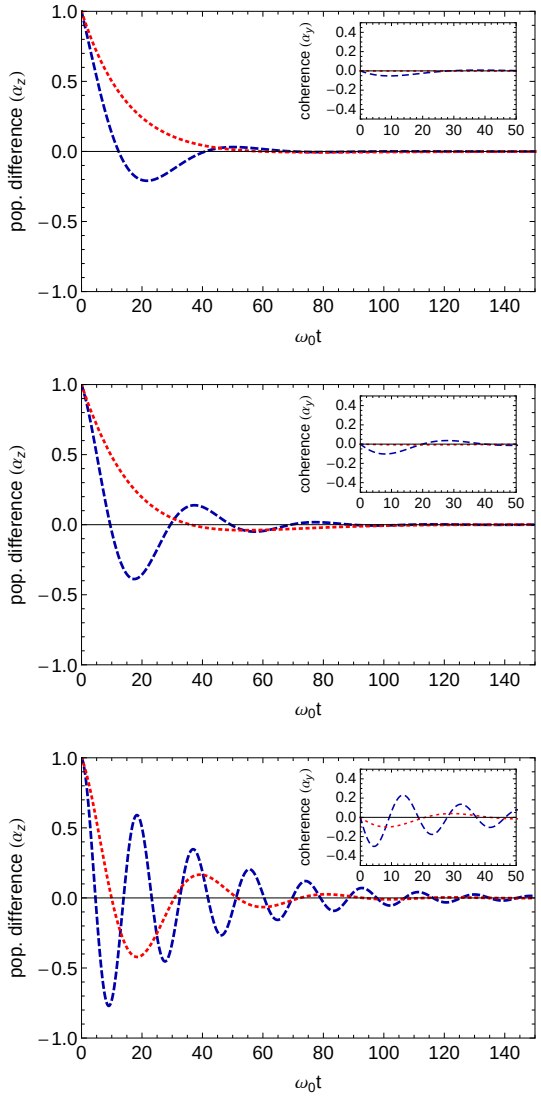


FIG. 2: Population difference as a function of scaled time $\omega_0 t$ for temperatures of $k_B T/\omega_0 = 5$ (blue dashed curves) and $k_B T/\omega_0 = 10$ (red dotted curves), and for separations corresponding to no correlation, $\mu = c/d\omega_0 = 0$ (top), weak correlations, $\mu = 0.5$ (middle), and strong correlations $\mu = 2$ (bottom). The insets show the evolution of the corresponding coherence $\alpha_y$. Parameters: $\alpha = 0.05$, $V/\omega_0 = 0.5$, and $\omega_c/\omega_0 = 4$.

also be used to elucidate the behaviour in which we are interested in general.[53] The cut-off frequency $\omega_c$ is needed to ensure that vacuum contributions remain finite, and is related to parameters specific to the particular physical system one wishes to model. To take our quantum dot example once more, in that system $\omega_c$ is essentially set by the localisation length of carriers within the dot region.[67] The inverse cut-off frequency also sets a typical relaxation timescale for the bath.[25]

To illustrate the dynamics and crossover behaviour in the resonant case, in Fig. 1 we plot the population difference ($\alpha_z$) as a function of the scaled time $\omega_0 t$ for a range of temperatures, showing the transition from coherent to incoherent transfer as the temperature is increased. In this plot, and all the following, we consider three-dimensional coupling, $F_3(\omega, d) = \mathrm{sinc}(\omega d/c)$. The role of bath spatial correlations in protecting coherence can be seen in Fig. 2, where we again plot the evolution of the population difference (the insets show the corresponding coherence $\alpha_y$), this time for representative intermediate and high-temperature cases. The different plots in Fig. 2 correspond to zero correlations, characterised by $\mu = c/d\omega_0 = 0$ ($d \to \infty$, top), weak correlations, $\mu = 0.5$ (middle), and strong correlations $\mu = 2$ (botttom).[75] Progressing from the uppermost plot to the lowest, we clearly see that an increase in correlation strength prolongs the timescale over which oscillations in both the population difference and coherence persist. Moreover, by looking at the curves corresponding to the higher temperature, we can see that as the degree of correlation is increased from zero, the dynamics moves from a regime showing purely incoherent relaxation, to a regime which displays coherent oscillations *at the same temperature*. The increase in correlations is thus able to extend the region of parameter space which permits coherence,[11] as we shall now explore in greater detail.

### A. Coherent to incoherent transition

We now return our attention to the crossover from coherent to incoherent transfer, defined by Eq. (31). Intuitively, we might expect the dynamics in the low-temperature (or weak-coupling) regime to be coherent; for example, in Fig. 1 incoherent relaxation only occurs in the high-temperature limit. If we therefore assume that the crossover itself occurs in the high-temperature regime, it is possible to derive an analytic expression governing the crossover temperature by approximating the rates $\Gamma_y$ and $\Gamma_z$. Details of this approximation, and its range of validity, can be found in the Appendix. Generally, for high enough temperatures and/or strong enough system-bath coupling (such that $\beta V_R \ll 1$) we can approximate $\gamma_{xx}(\eta) \approx \gamma_{yy}(\eta) \approx \gamma_{yy}(0)$ in $\Gamma_y$ and $\Gamma_z$, where

$$\gamma_{yy}(0) \approx \frac{\beta B^2 \mathrm{e}^{\phi_0 C_0(x,y)}}{2\sqrt{\pi C_2(x,y)\phi_0}}, \tag{33}$$

with $\phi_0 = 2\pi^2\alpha/\omega_0^2\beta^2$, $x = \pi d/c\beta$ and $y = \omega_c\beta$. The functions $C_0(x,y)$ and $C_2(x,y)$ are given by Eqs. (A7) and (A8), and the renormalisation factor $B$ by the product of Eqs. (A14) and (A15). If we further assume that the energy shift $\lambda_3$ vanishes in the high-temperature limit, Eq. (31) reduces to

$$(\Gamma_z - \Gamma_y) = 4V_R, \tag{34}$$

and we arrive at the expression

$$\left(\frac{k_B T}{\omega_0}\right)^2 = \frac{V}{\omega_0}\frac{B\mathrm{e}^{\phi_0 C_0(x,y)}}{4\sqrt{2\pi^3\alpha C_2(x,y)}}, \tag{35}$$

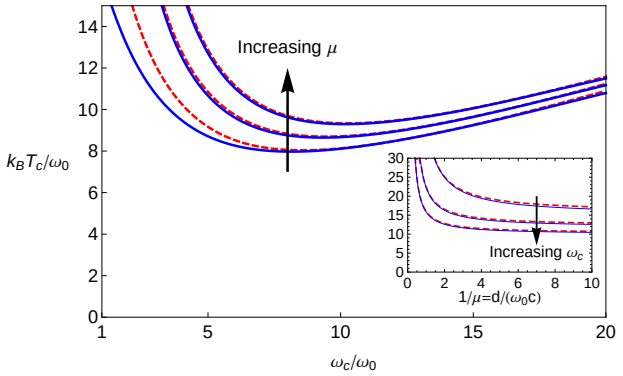


FIG. 3: Crossover temperature separating the coherent and incoherent regimes against cut-off frequency, for levels of correlation given by $\mu = c/d\omega_0 = 0$, $\mu = 0.5$ and $\mu = 1$, increasing as shown. The solid blue curves have been calculated from Eq. (31) (using the full rates), while the dashed red curves are solutions to the high-temperature approximation, Eq. (35). The inset shows the dependence on the level of correlation ($1/\mu = d/(\omega_0 c)$) for different cutoffs, $\omega_c/\omega_0 = 2$, $\omega_c/\omega_0 = 3$, and $\omega_c/\omega_0 = 4$, again increasing as shown. Parameters: $\alpha = 0.05$ and $V/\omega_0 = 0.5$.

with solution, $T_c$, giving the crossover temperature separating the coherent and incoherent regimes.

The dependence of $T_c$ on the various parameters involved in the problem is not straightforward, owing to the temperature dependence in the renormalisation factor $B$, in the functions $C_0$ and $C_2$, and in $\phi_0$. In fact, there are three distinct and important temperature scales: $T_0 = \omega_0/(\sqrt{2\alpha}\pi k_B)$, which depends upon the system-bath coupling strength; $T_x = c/d\pi k_B$, which arises due to the fluctuation correlations and becomes unimportant in the uncorrelated case ($T_x \to 0$ as $d \to \infty$); and $T_y = \omega_c/k_B$, dependent upon the cut-off frequency, and irrelevant in the scaling limit ($y \to \infty$). Hence, changes in any of $\alpha$, $d$, or $\omega_c$ can have an effect on the crossover temperature. For example, the main part of Fig. 3 shows the solution to Eq. (35), i.e. the crosover temperature $T_c$, as a function of the dimensionless cut-off frequency $\omega_c/\omega_0$. A calculation using Eq. (31) with the full rates, and including $\lambda_3$, is also shown for comparison. The three pairs of curves correspond to increasing levels of correlation, ordered as indicated. We see that, except for small $\omega_c/\omega_0$ in the case $\mu = 0$, where $\lambda_3$ becomes important, solutions to Eq. (35) give an excellent approximation to the crossover temperature calculated using the full rates. This confirms that the coherent-incoherent crossover does indeed occur in the high-temperature (multiphonon) regime, and consequently could not be captured by a weak system-bath coupling treatment.

As the cut-off frequency is increased from its minimum value, the crossover temperature begins to decrease. This behaviour can be understood qualitatively by examining Eq. (34), and considering the competition this condition captures between the rate $\Gamma_z - \Gamma_y$ and the coherent interaction $V_R$ in defining the nature of the dynamics. Larger values of the cut-off frequency correspond to smaller values of the renormalised interaction strength $V_R$ (see e.g. Eq. (A14)), while the rates $\Gamma_y$ and $\Gamma_z$ vary less strongly with $\omega_c$ in this regime. Thus, increasing $\omega_c$ from its minimum value decreases $V_R$, and therefore reduces the range of temperatures for which $4V_R > \Gamma_z - \Gamma_y$ and coherent transfer can take place. Thus, the crossover temperature falls. Physically, this can be understood by noting that as the cut-off frequency is increased, so too is the effective frequency range and peak magnitude of the system-bath interaction, characterised by the spectral density [Eq. (32)]. Hence, increasing from small $\omega_c/\omega_0$, the environment begins to exert an enhanced influence on the system behaviour, and so coherent dynamics no longer survives to such high temperatures. As $\omega_c$ continues to increase, however, we see the crossover temperature then begins to rise. The renormalisation factor $B$ tends to zero with increasing $\omega_c$ and here becomes the dominating quantity, thus causing the rate $\Gamma_z - \Gamma_y \sim \mathcal{O}(B^2)$ to vanish faster than the renormalised donor-acceptor coupling $V_R = BV$.

The interplay between the size of $\omega_c$ and the level of spatial correlation is best understood by considering the inset of Fig. 3. For all curves shown the crossover temperature increases as the distance $d$ is reduced, since the level of correlation $\mu$ increases correspondingly. As we have seen previously in Fig. 2, stronger correlations allow coherent dynamics to be observed at higher temperatures; since environmental effects are suppressed, so the crossover temperature $T_c$ must rise. This behaviour can be attributed to an increase in the renormalised interaction strength, $V_R$, in relation to the rate $\Gamma_z - \Gamma_y$, this time with variations in the correlation level $\mu$. Interestingly, as the cut-off frequency is increased up to $\omega_c/\omega_0 = 4$ (lowest curve), we see that not only does the crossover temperature decrease, but also that the degree of correlation necessary to show a marked rise in $T_c$ increases. As can be seen by comparing the separation between the different curves in the main part of the figure, increasing the cut-off frequency tends to suppress the extent to which correlations are able to protect coherence in the system. This tallies with the dynamics shown in Fig. 2, for which $\omega_c/\omega_0 = 4$, and correlations as high as $\mu = 2$ were needed before a significant change in behaviour was seen. Finally, since the renormalisation factor $B$ tends to a constant non-zero value as the correlations vanish at large $d$ (as opposed to $B \to 0$ as $\omega_c \to \infty$), the dependence of the crossover temperature on $\mu$ is monotonic, in contrast to its dependence on $\omega_c$.

## IV. OFF RESONANCE

It is often the case in practice that the donor and acceptor will have different excited state energies, $\epsilon_1 - \epsilon_2 = \epsilon \neq 0$, and so we now turn our attention to energy transfer dynamics under off-resonant conditions. Regarding the

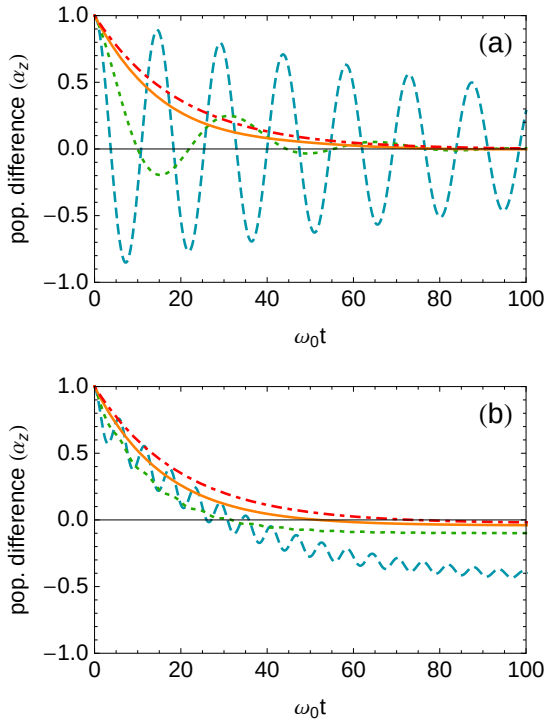


FIG. 4: Population difference for (a) small energy mismatch ($\epsilon/\omega_0 = 0.1$) and (b) larger energy mismatch ($\epsilon/\omega_0 = 1$) as a function of scaled time $\omega_0 t$. Temperatures $k_B T/\omega_0 = 1$ (blue dashed curve), $k_B T/\omega_0 = 5$ (green dotted curve), $k_B T/\omega_0 = 12$ (orange solid curve) and $k_B T/\omega_0 = 20$ (red dot-dashed curve) are shown. Parameters: $\alpha = 0.05$, $V/\omega_0 = 0.5$, $\omega_c/\omega_0 = 4$, and $\mu = 0.5$.

coherent to incoherent transition, in the resonant case we were able to identify this point with a pair of conjugate eigenvalues converging on the real axis, thus changing oscillatory terms into relaxation. We might hope that in the off-resonant case we are able to establish a similar crossover criterion, and again use this to investigate the effects of bath correlations and the cut-off frequency. However, we shall see that such an identification is less straightforward in the off-resonant regime.

We first present the full Bloch equations describing the evolution of our donor-acceptor pair for arbitrary energy mismatch. As in the resonant case, we have an equation of motion of the form $\dot{\boldsymbol{\alpha}} = M \cdot \boldsymbol{\alpha} + \boldsymbol{b}$, but now the matrix $M$ is given by

$$M = \begin{pmatrix} -\Gamma_x & -(\epsilon + \lambda_1) & 0 \\ (\epsilon + \lambda_2) & -\Gamma_y & -2BV_R \\ B^{-1}\zeta & B^{-1}(2V_R + \lambda_3) & -\Gamma_z \end{pmatrix}, \quad (36)$$

with $\boldsymbol{b} = (-B\kappa_x, -B\kappa_y, -\kappa_z)^T$, and the more complicated expressions

$$\Gamma_x = V^2(\gamma_{yy}(\eta) + \gamma_{yy}(-\eta)), \quad (37)$$

$$\Gamma_y = 2V^2\left(\frac{4V_R^2}{\eta^2}\gamma_{xx}(0) + \frac{\epsilon^2}{2\eta^2}(\gamma_{xx}(\eta) + \gamma_{xx}(-\eta))\right), \quad (38)$$

$$\Gamma_z = \Gamma_x + \Gamma_y, \quad (39)$$

$$\lambda_1 = \frac{2V^2\epsilon}{\eta}(S_{yy}(\eta) - S_{yy}(-\eta)), \quad (40)$$

$$\lambda_2 = \frac{2V^2\epsilon}{\eta}(S_{xx}(\eta) - S_{xx}(-\eta)), \quad (41)$$

$$\lambda_3 = \frac{4V^2V_R}{\eta}(S_{yy}(\eta) - S_{yy}(-\eta)), \quad (42)$$

$$\zeta = \frac{4V^2V_R\epsilon}{\eta^2}\left(\gamma_{xx}(0) - \frac{1}{2}(\gamma_{xx}(\eta) + \gamma_{xx}(-\eta))\right), \quad (43)$$

$$\kappa_x = \frac{2V^2V_R}{\eta}(\gamma_{yy}(\eta) - \gamma_{yy}(-\eta)), \quad (44)$$

$$\kappa_y = \frac{8V^2V_R\epsilon}{\eta^2}\left(S_{xx}(0) - \frac{1}{2}(S_{xx}(\eta) + S_{xx}(-\eta))\right), \quad (45)$$

$$\kappa_z = \frac{V^2\epsilon}{\eta}\left((\gamma_{xx}(\eta) - \gamma_{xx}(-\eta)) + (\gamma_{yy}(\eta) - \gamma_{yy}(-\eta))\right). \quad (46)$$

Here, $\eta = \sqrt{\epsilon^2 + 4V_R^2}$ is the system Hamiltonian eigenstate splitting in the polaron frame.

To exemplify the dynamics generated by the full Bloch equations, in Fig. 4 we plot the evolution of the population difference in the case of (a) a small donor-acceptor energy mismatch, $\epsilon = 0.2V$, and (b) a more substantial mismatch, $\epsilon = 2V$. By comparison of Fig. 1 (plotted in the resonant case) and Fig. 4(a), we see that the introduction of a small energy mismatch has only a marginal effect on the dynamics, and most importantly the coherent or incoherent nature of the energy transfer process seems unaffected. In contrast, in Fig. 4(b) the presence of a larger energy mismatch causes the low-temperature oscillations to increase in frequency but decrease markedly in amplitude, such that for $k_B T/\omega_0 = 5$ oscillations are now almost imperceptible. We also see that the population difference tends to a non-zero steady-state at low temperatures, as we might expect from simple thermodynamic arguments, since the states $\alpha_z = 1$ and $\alpha_z = -1$ now have different energies. As the temperature is raised, however, the dynamics still looks to be approaching that shown in the resonant case of Fig. 1.

Finding the eigensystem of the off-resonant $M$ [Eq. (36)] is not straightforward and analytical solutions to the full Bloch equations are consequently lengthy, and therefore of little direct use in gaining an understanding of the behaviour seen in Fig. 4. A large part of this section is thus devoted to deriving simplified expressions for the energy transfer dynamics in a number of limits. These expressions not only provide insight into the off-resonant behaviour of the system, but also serve to highlight the difficultly in now defining a simple crossover

criterion, as was possible in the resonant case.

### A. Near Resonance

We have seen that when only a small donor-acceptor energy mismatch was introduced, we observed very little difference to the resonant dynamics. This is to be expected, as the interaction $V$ still dominates over $\epsilon$ in this regime, i.e. $\epsilon/V \ll 1$. To show this analytically, we note that provided we are sufficiently within this limit, the dynamics generated by $\epsilon$ is also much slower than the dissipative processes we wish to capture, and we can simply add a term

$$E = \begin{pmatrix} 0 & -\epsilon & 0 \\ \epsilon & 0 & 0 \\ 0 & 0 & 0 \end{pmatrix} \tag{47}$$

to $M_R$ of Eq. (17), reducing our problem to solving $\dot{\boldsymbol{\alpha}}' = (M_R + E) \cdot \boldsymbol{\alpha}'$. Hence, the arguments presented in Section II C tell us that the characteristics of the energy transfer process can be found simply by analysing the eigenspectrum of $M_R + E$. On resonance ($\epsilon = 0$) the eigenvectors and eigenvalues of $M_R$ are given by Eqs. (25), (26) and (27), together with the accompanying text. By diagonalisation of $M_R + E$ for small energy mismatch, we find that to first order in $\epsilon$ these eigenvalues are unchanged. To second order in $\epsilon$ the eigenvalues have corrections

$$\Delta q_1 = -\frac{4\epsilon^2 \Gamma_y}{(3\Gamma_y - \Gamma_z)^2 + \xi_R^2}, \tag{48}$$

$$\Delta q_2 = -\frac{i\epsilon^2}{\xi_R}\left(\frac{(\Gamma_y - \Gamma_z)(3\Gamma_y - \Gamma_z) + 2i\xi_R\Gamma_y + \xi_R^2}{(3\Gamma_y - \Gamma_z)^2 + \xi_R^2}\right), \tag{49}$$

and $\Delta q_3 = \Delta q_2^*$. The change $\Delta q_1$ is always real since the rates $\Gamma_z$ and $\Gamma_y$ are real by construction and $\xi_R$ can be either purely real or purely imaginary. Inspection of the expression for $\Delta q_2$ reveals that is has real and imaginary components when $\xi_R$ is real (in which case $q_2$ also has both real and imaginary parts), and is entirely real if $\xi_R$ is imaginary (in which case $q_2$ is also real). Put another way, the second order (in $\epsilon$) correction to the eigenvalues $q_2$ and $q_3$ does not change whether they lie on the real axis or otherwise. Recalling that a complex $q_2$ and $q_3$ (or real $\xi_R$) corresponds to coherent dynamics, we confirm that the introduction of a small energy difference between the two sites does not affect whether the energy transfer process is of a coherent or an incoherent nature.

### B. Weak-coupling limit

Let us now move beyond the small $\epsilon$ approximation and look instead at the weak system-bath coupling limit, which we obtain by expanding all relevant quantities to first order in $J(\omega)$. With reference to our expressions for the correlation functions [Eqs. (11) and (12)], we see that within this approximation $\Lambda_{xx}(\tau) \to 0$ while $\Lambda_{yy}(\tau)$ remains finite. We may then set to zero all rates and energy shifts which are functions of $\Lambda_{xx}(\tau)$ only in Eq. (36). This results in the far simpler form

$$M_W = \begin{pmatrix} -\Gamma_W & -(\epsilon + \lambda_1) & 0 \\ \epsilon & 0 & -2BV_R \\ 0 & B^{-1}(2V_R + \lambda_3) & -\Gamma_W \end{pmatrix}, \tag{50}$$

where the weak-coupling rate is given by[68]

$$\Gamma_W = 4\pi\left(\frac{V_R}{\eta}\right)^2 J(\eta)(1 - F(\eta, d)) \coth(\beta\eta/2), \tag{51}$$

and the two energy shifts may be written $\lambda_1 = (\epsilon/\eta)\Lambda$ and $\lambda_3 = (2V_R/\eta)\Lambda$, with

$$\Lambda = 2V^2(S_{yy}(\eta) - S_{yy}(-\eta)). \tag{52}$$

The inhomogeneous term becomes $\boldsymbol{b}_W = \{-B\kappa_x, 0, -(\epsilon/2V_R)\kappa_x\}^T$ in the same limit, which leads to the weak-coupling steady state

$$\alpha_x(\infty) = -\frac{2BV_R}{\eta}\tanh(\beta\eta/2), \tag{53}$$

$$\alpha_y(\infty) = 0, \tag{54}$$

$$\alpha_z(\infty) = -\frac{\epsilon}{\eta}\tanh(\beta\eta/2). \tag{55}$$

As in the resonant case (in which there was no weak-coupling approximation), this steady-state has precisely the form as that expected from a standard weak-coupling approach, though with the replacement $V \to V_R$, and the extra factor of $B$ suppressing the coherence $\alpha_x(\infty)$. As the energy mismatch increases in relation to $V$, the weak-coupling steady state therefore becomes increasingly localised in the lower energy state $|1\rangle \equiv |GX\rangle$. Interestingly, this contrasts with the qualitatively incorrect form (at low temperatures at least) given by the Non-Interacting Blip Approximation (NIBA), $\alpha_z^{\mathrm{NIBA}}(\infty) = -\tanh(\beta\epsilon/2)$,[66,69] which predicts complete localisation in the lower energy state at zero temperature, regardless of the size of $\epsilon/V$. We should thus expect the present theory to fair far better than the NIBA for low-temperatures (or weak-coupling) in the off-resonant case, $\epsilon \neq 0$. The rate $\Gamma_W$ given in Eq. (51) is also of the form expected from a weak-coupling treatment, though once more with the renormalisation $V \to V_R$. In fact, such a replacement is sometimes made by hand in weak-coupling theories to provide agreement with numerics over a larger range of parameters,[68] though it arises naturally in the polaron formalism here. We can therefore conclude that, in addition to allowing for the exploration of multiphonon effects,[11,12,51,55] the polaron master equation also provides a rigorous way to explore the (single-phonon) weak-coupling regime for spectral densities of the type in Eq. (32).[51]

As before, to find the time evolution of $\boldsymbol{\alpha}$ we evaluate the eigensystem of $M_W$. For $\epsilon \neq 0$, we find eigenvectors

$$\boldsymbol{m}_1 = \left\{\frac{2BV_R}{\epsilon}, 0, 1\right\}^T, \tag{56}$$

$$\boldsymbol{m}_2 = \boldsymbol{m}_3^* = \left\{\frac{B}{\epsilon}\left(2V_R - \frac{\eta^2}{2V_R}\right), \frac{B(\Gamma_W - i\xi_{\rm W})}{2(2V_R+\lambda_3)}, 1\right\}^T, \tag{57}$$

with corresponding eigenvalues $q_1 = -\Gamma_W$, $q_2 = q_3^* = -(1/2)(\Gamma_W + i\xi_{\rm W})$, and weak-coupling oscillation frequency

$$\xi_{\rm W} = \sqrt{4\eta(\eta+\Lambda) - \Gamma_W^2}, \tag{58}$$

which we should expect to be real to be consistent with our original expansion. We immediately see that, in general, the off-resonant dynamics in the weak-coupling limit should have a different form to the resonant dynamics. In fact, Eqs. (56) and (57) show that, in contrast to the resonant case, the population evolution should have two distinct contributions. This can be made explicit by considering the initial state $\boldsymbol{\alpha}(0) = \{0, 0, 1\}^T$, for which we obtain

$$\begin{aligned}\alpha_z(t) &= \frac{\epsilon}{\eta}\left(\frac{\epsilon}{\eta}{\rm e}^{-\Gamma_W t} - \left(1 - {\rm e}^{-\Gamma_W t}\right)\tanh(\beta\eta/2)\right) \\ &\quad + \frac{4V_R^2}{\eta^2}{\rm e}^{-\frac{\Gamma_W t}{2}}\left(\cos\left(\frac{\xi_{\rm W} t}{2}\right) - \frac{\Gamma_W}{\xi_{\rm W}}\sin\left(\frac{\xi_{\rm W} t}{2}\right)\right).\end{aligned} \tag{59}$$

Here, the first term, proportional to $(\epsilon/\eta)$ and present nowhere in the resonant case, describes incoherent relaxation towards the steady state value given by Eq. (55). The second term, proportional to $(V_R/\eta)^2$ and having a similar form to the resonant dynamics, describes damped oscillations with frequency $\xi_W$. Importantly, these oscillations have a temporal maximum amplitude of $4V_R^2/\eta^2 \leq 1$, compared to 1 in the resonant case. The effect of the energy mismatch in this limit is thus to suppress the amplitude of any oscillations in the population difference, while increasing their frequency due to the dependence of $\xi_W$ on $\eta$ in Eq. (58), exactly as seen in Fig. 4(b).

### C. High temperature (or far from resonance) limit

By taking appropriate limits, we have now been able to explain the behaviour seen at small $\epsilon$ and at low temperatures in Fig. 4. However, at higher temperatures, we find something quite different; the population dynamics appears to be relatively insensitive to the size of the energy mismatch. In order to investigate this effect in more detail, we shall now make a high-temperature (or strong system-bath coupling) approximation to the full energy transfer dynamics.

Specifically, we consider the regime $V_R/\epsilon \ll 1$. This limit can in fact be achieved in two possible ways. Firstly, recalling that $V_R = BV$, we see that $V_R$ can be made small by increasing the system-bath coupling strength or temperature, such that $B \ll 1$. Alternatively, if the donor-acceptor pair are far from resonance, the ratio $V/\epsilon$ will be small, and hence $V_R/\epsilon$ smaller still. Observing that the correlation functions given by Eqs. (11) and (12) are both proportional to $B^2$, we can see that all dissipative terms in the equation of motion, $\dot{\boldsymbol{\alpha}} = M \cdot \boldsymbol{\alpha} + \boldsymbol{b}$, are at least of order $V_R^2$. We proceed by keeping only terms up to order $(V_R/\epsilon)^2$ in the full off-resonant $M$ and $\boldsymbol{b}$. This allows us to set $\lambda_3$, $\zeta$, $\kappa_x$ and $\kappa_y$ to zero, while the remaining quantities reduce to

$$\Gamma_y = V^2(\gamma_{xx}(\eta) + \gamma_{xx}(-\eta)), \tag{60}$$

$$\Gamma_z = V^2\big(\gamma_{xx}(\eta) + \gamma_{xx}(-\eta) + \gamma_{yy}(\eta) + \gamma_{yy}(-\eta)\big), \tag{61}$$

$$\lambda_1 = 2V^2(S_{yy}(\eta) - S_{yy}(-\eta)), \tag{62}$$

$$\lambda_2 = 2V^2(S_{xx}(\eta) - S_{xx}(-\eta)), \tag{63}$$

$$\kappa_z = V^2\big(\gamma_{xx}(\eta) - \gamma_{xx}(-\eta) + \gamma_{yy}(\eta) - \gamma_{yy}(-\eta)\big). \tag{64}$$

Hence, in the high-temperature limit, Eq. (36) takes on the simpler form

$$M_{\rm HT} = \begin{pmatrix} -(\Gamma_z - \Gamma_y) & -(\epsilon + \lambda_1) & 0 \\ (\epsilon + \lambda_2) & -\Gamma_y & -2BV_R \\ 0 & 2B^{-1}V_R & -\Gamma_z \end{pmatrix}, \tag{65}$$

while the inhomogeneous term reduces to $\boldsymbol{b}_{\rm HT} = \{0, 0, -\kappa_z\}^T$. We then find the approximate steady-state

$$\alpha_x(\infty) = -\frac{2BV_R}{\epsilon}\tanh(\beta\eta/2), \tag{66}$$

$$\alpha_y(\infty) = 0, \tag{67}$$

$$\alpha_z(\infty) = -\left(1 + \frac{4V_R^2}{\epsilon^2}\left(\frac{\Gamma_y}{\Gamma_z} - 1\right)\right)\tanh(\beta\eta/2), \tag{68}$$

valid up to second order in $V_R/\epsilon$. For $V_R \ll \epsilon$, the steady-state is strongly localised in the low energy state ($\alpha_z(\infty) \approx -1$) if $\epsilon \gg k_B T$, though for $\epsilon \ll k_B T$ thermal effects dominate and $\alpha_z(\infty) \approx 0$ as in the resonant case. Again, this behaviour tallies with Fig. 4.

To obtain the corresponding population dynamics, we note in reference to Eq. (16) that the coefficients $a_i$, the eigenvectors $\boldsymbol{m}_i$, and the eigenvalues $q_i$ will contain powers of our expansion parameter $V_R/\epsilon$. Expanding both $q_i$ and the products $a_i\boldsymbol{m}_i$ to second order, we find

$$\begin{aligned}\alpha_z(t) &= {\rm e}^{-\Gamma_z t}\left(1 - \frac{4V_R^2}{\epsilon^2}\right) + \frac{4V_R^2}{\epsilon^2}{\rm e}^{-\Gamma_z t/2}\cos(\bar{\epsilon} t) \\ &\quad -(1 - {\rm e}^{-\Gamma_z t})\tanh\left(\frac{\beta\eta}{2}\right)\left[1 + \frac{4V_R^2}{\epsilon^2}\left(\frac{\Gamma_y}{\Gamma_z} - 1\right)\right]\end{aligned} \tag{69}$$

where the shifted oscillation frequency is

$$\bar{\epsilon} = \epsilon + (1/2)(\lambda_1 + \lambda_2) + 2\epsilon(V_R/\epsilon)^2. \tag{70}$$

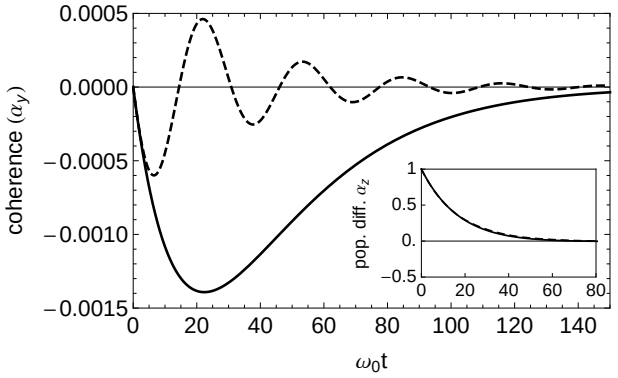


FIG. 5: Coherence ($\alpha_y$) as a function of scaled time $\omega_0 t$ for resonant ($\epsilon = 0$, solid curve) and off-resonant ($\epsilon/\omega_0 = 0.2$, dashed curve) cases. The temperature, $k_B T/\omega_0 = 13$, is chosen to be above the relevant crossover $T_c$ in the resonant case, such that the resonant dynamics is guaranteed to be incoherent. Parameters: $\alpha = 0.05$, $V/\omega_0 = 0.5$, $\omega_c/\omega_0 = 4$, and $\mu = 0.5$. The inset shows the corresponding population dynamics.

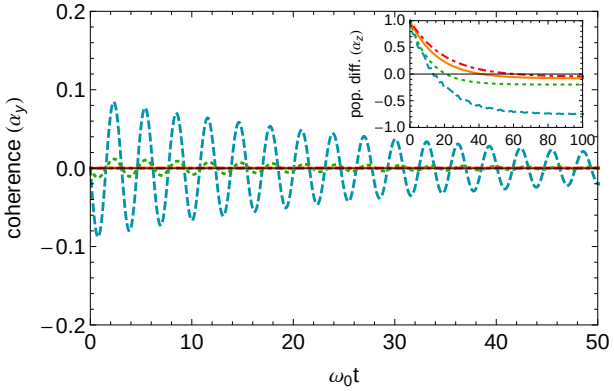


FIG. 6: Coherence ($\alpha_y$) as a function of scaled time $\omega_0 t$ for temperatures of $k_B T/\omega_0 = 1$ (blue dashed curve), $k_B T/\omega_0 = 5$ (green dotted curve), $k_B T/\omega_0 = 12$ (orange solid curve) and $k_B T/\omega_0 = 20$ (red dot-dashed curve). Parameters: $\alpha = 0.05$, $V/\omega_0 = 0.5$, $\omega_c/\omega_0 = 4$, $\epsilon/\omega_0 = 2$ and $\mu = 0.5$. The inset shows the corresponding population dynamics.

As in the weak-coupling case [Eq. (59)] the evolution of the donor-acceptor population difference consists of two contributions; incoherent relaxation towards the steady-state, and an oscillatory component with vanishing amplitude as $V_R/\epsilon \to 0$. The energy mismatch again serves to suppress oscillations in the population difference.

The most striking feature, however, of the Eq. (69) is that there is an oscillatory component at frequency $\bar{\epsilon}$ at all. In the high-temperature limit, we might expect that this frequency would reach a point where it becomes imaginary and $\alpha_z(t)$ displays purely incoherent relaxation, as in the equivalent resonant case. However, we can see that this is clearly not the case since $\bar{\epsilon}$ is always real by definition. Furthermore, at very high temperatures $\bar{\epsilon} \to \epsilon$, and it therefore also remains finite. Eq. (69) thus highlights an important difference between the energy transfer dynamics in resonant and off-resonant situations. In the resonant case, as temperature is increased, the energy transfer process becomes less coherent through a reduction in oscillation frequency (i.e. $V_R$ becomes small in comparison to $\Gamma_z - \Gamma_y$), eventually reaching a point at which population relaxes incoherently towards the steady state. In the off-resonant case, the transfer process becomes less coherent predominately through a reduction in oscillation amplitude. For high temperatures, an oscillatory component is still (in theory) present in the system, although it becomes ever more dominated by incoherent relaxation towards the steady-state population distribution, which depends upon the ratio $\epsilon/k_B T$. These features are clearly seen in Fig. 4.

Only to first order in $V_R/\epsilon$ do our expressions predict purely incoherent off-resonant population transfer:

$$\alpha_z(t) = \mathrm{e}^{-\Gamma_z t} - (1 - \mathrm{e}^{-\Gamma_z t}) \tanh(\beta\eta/2). \qquad (71)$$

Let us also consider the evolution of $\alpha_x$ and $\alpha_y$ in the same limit:

$$\alpha_x(t) = \frac{2BV_R}{\epsilon}\Big(\mathrm{e}^{-\Gamma_z t} - (1 - \mathrm{e}^{-\Gamma_z t}) \tanh(\beta\eta/2) - \mathrm{e}^{-(1/2)\Gamma_z t} \cos(\bar{\epsilon} t)\Big), \qquad (72)$$

$$\alpha_y(t) = -\frac{2BV_R}{\epsilon} \mathrm{e}^{-(1/2)\Gamma_z t} \sin(\bar{\epsilon} t). \qquad (73)$$

Hence, although the donor-acceptor population itself evolves entirely incoherently in this limit, the coherences may still perform oscillations due to the energy mismatch. To illustrate the difference in the transition to incoherent population transfer on- and off-resonance, in the main part of Fig. 5 we plot the evolution of the coherence $\alpha_y(t)$ in both cases. The parameters have been chosen such that the resonant dynamics is in the incoherent regime ($T > T_c$), hence the resonant $\alpha_y$ displays no oscillations [see Eq. (29)]. In accordance with Eq. (73), however, the introduction of an energy mismatch induces oscillations in the donor-acceptor coherence. While these oscillations have an almost negligible amplitude, this behaviour serves to illustrate the subtlety in defining a strict crossover from coherent to incoherent dynamics in the off-resonant case. In particular, despite the different forms of coherence behaviour, the corresponding (essentially incoherent) population dynamics shown in the inset is almost indistinguishable in the two cases, even though there should still be a strongly suppressed coherent contribution in the off-resonant curve.

An alternative way to obtain coherence oscillations in a regime of predominantly incoherent population transfer is to introduce a large energy mismatch (i.e. make $V/\epsilon$ small) at low temperature, as shown in Fig. 6. Here, for the lowest temperature considered the population relaxes towards its steady state value with little sign of oscillation, while the coherence performs oscillations with a

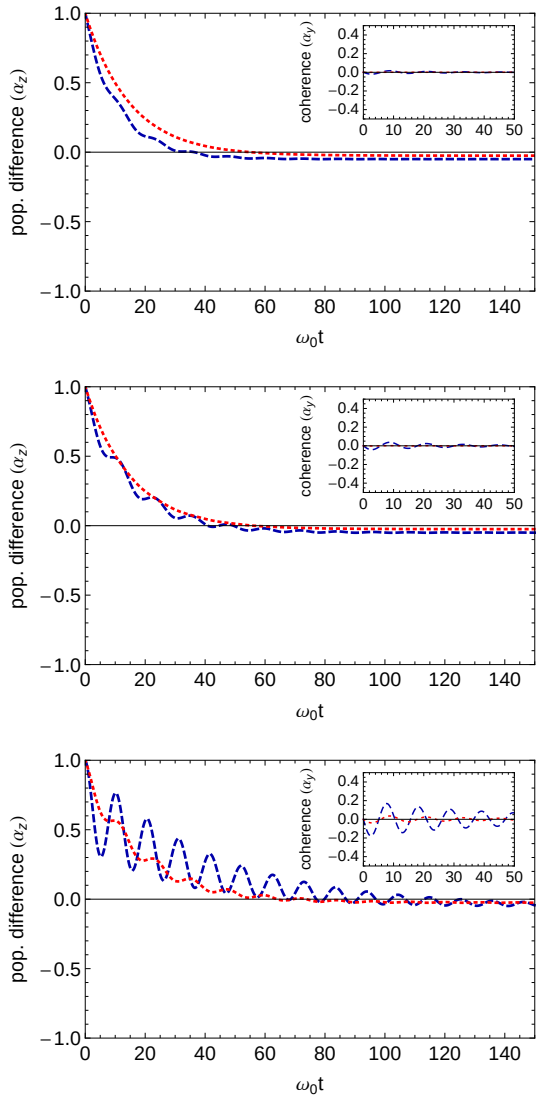


FIG. 7: Population difference as a function of scaled time $\omega_0 t$ for temperatures of $k_B T/\omega_0 = 5$ (blue dashed curve) and $k_B T/\omega_0 = 10$ (red dotted curve), and for separations corresponding to no fluctuation correlations, $\mu = c/d\omega_0 = 0$ (top), weak correlations, $\mu = 0.5$ (middle) and strong correlations $\mu = 2$ (botttom). The insets show the evolution of the corresponding coherence $\alpha_y$. Parameters: $\alpha = 0.05$, $V/\omega_0 = 0.5$, $\epsilon/\omega_0 = 0.5$, and $\omega_c/\omega_0 = 4$.

significant amplitude and considerable lifetime. This behaviour is strongly suppressed, however, as temperature increases, such that $k_B T > \epsilon$.

### D. Correlated fluctuations

We have seen in the previous sections that for off-resonant energy transfer the distinction between coherent and incoherent dynamics is less easily defined than in the resonant case. However, we should still expect changes in the level of correlation in the donor and acceptor fluctuations to have a similar effect on the transfer process.

To illustrate that this is indeed the case, in Fig. 7 we plot the donor-acceptor population dynamics in off-resonant conditions for three different levels of fluctuation correlation (increasing from top to bottom). Just as we found in the resonant case of Fig. 2, an increase in correlations enhances the lifetime of coherence present in the energy transfer process. In addition, in the off-resonant case stronger correlations also serve to amplify the coherent contribution to the full energy transfer dynamics, since the renormalised interaction strength $V_R$ increases in relation to the energy mismatch $\epsilon$.

## V. SUMMARY

Motivated by recent experiments which suggest that quantum coherence can survive in energy transfer processes even under potentially adverse environmental conditions,[1–9] we have investigated various factors that determine the nature of the energy transfer dynamics in a model donor-acceptor pair. To do so, we used a polaron transform, Markovian master equation technique.[11] This formalism is attractive as it allows for exploration of both the low-temperature (or weak-coupling) and high-temperature (or strong-coupling) regimes, as well as reliable interpolation between these two limits, provided $V/\omega_c$ does not become large.[13,51,55] We are also able to consistenly describe off-resonant effects, unlike in the NIBA,[66,69] and the influence of bath correlations.

In the resonant case we identified a crossover temperature separating coherent and incoherent energy transfer. We found a non-trivial dependence of this temperature on both the degree of spatial correlation within the bath-induced fluctuations, and also on the cut-off frequency of the bath spectral density. Smaller cut-off frequencies were also found to enhance the extent to which bath spatial correlations are able to protect coherence in the system. The crossover generally occurs in a high-temperature limit where multiphonon effects dominate, and so could not be captured by a standard perturbative treatment of the system-bath interaction.

In the off-resonant case we found that coherent and incoherent regimes are less easily defined. In particular, for a sufficiently large energy mismatch between the donor and acceptor, coherence can in theory be present at all but infinite temperatures, albeit with an ever decreasing amplitude. However, using analytic expressions derived in various limits, we were able to characterise the off-resonant energy transfer process over much of the parameter space, illustrating the suppression of coherence in the population dynamics with increasing temperature or energy mismatch. We also showed that strong correlations have a qualitatively similar effect to the resonant case, protecting coherence in the transfer process.

While we have concentrated in this work on elucidating general features of donor-acceptor energy transfer dy-

namics using a simple model system, the insight we have gained could be relevant to a variety of systems. In addition to those already mentioned,[1–9] closely-spaced pairs of semiconductor quantum dots could provide a solid-state implementation of the model studied here.[70] In particular, our polaron master equation theory provides a bridge between the weak[68] and strong[71] system-bath coupling approximations already explored in this context. It would also be interesting to analyse the energy transfer dynamics of larger donor-acceptor complexes within the polaron formalism,[72] to see if further understanding of the interplay between coherent and incoherent processes in such systems could be obtained. Finally, it would be desirable to perform a thorough investigation of the regime of validity of the polaron approach by comparison to numerically exact techniques.[73]

### Acknowledgments

We are very grateful to Alexandra Olaya-Castro, Andrew Fisher, and Avinash Kolli for interesting discussions and useful comments. This research was supported by the EPSRC.

### Appendix A: High temperature rates

Here we show how to obtain analytic approximations for the decoherence rates at high temperatures by use of a saddle point integration. Within our formalism there are two rates which need to be evaluated:

$$\gamma_{xx}(\eta) = \frac{B^2}{2}\int_{-\infty}^{+\infty} \mathrm{d}\tau \mathrm{e}^{i\tau\eta}(\mathrm{e}^{\phi(\tau)} + \mathrm{e}^{-\phi(\tau)} - 2), \quad \text{(A1)}$$

$$\gamma_{yy}(\eta) = \frac{B^2}{2}\int_{-\infty}^{+\infty} \mathrm{d}\tau \mathrm{e}^{i\tau\eta}(\mathrm{e}^{\phi(\tau)} - \mathrm{e}^{-\phi(\tau)}), \quad \text{(A2)}$$

where $\phi(\tau)$ is given by Eq. (13). With the appropriate manipulations[51] it is possible to show that

$$\gamma_{xx}(\eta) = \frac{B^2}{2}\mathrm{e}^{\beta\eta/2}\int_{-\infty}^{+\infty} \mathrm{d}\tau \mathrm{e}^{i\tau\eta}(\mathrm{e}^{\tilde{\phi}(\tau)} + \mathrm{e}^{-\tilde{\phi}(\tau)} - 2), \quad \text{(A3)}$$

$$\gamma_{yy}(\eta) = \frac{B^2}{2}\mathrm{e}^{\beta\eta/2}\int_{-\infty}^{+\infty} \mathrm{d}\tau \mathrm{e}^{i\tau\eta}(\mathrm{e}^{\tilde{\phi}(\tau)} - \mathrm{e}^{-\tilde{\phi}(\tau)}), \quad \text{(A4)}$$

where now $\tilde{\phi}(\tau) = \tilde{\phi}(-\tau) = \phi(\tau - i\beta/2)$, and is given explicitly in integral form by

$$\tilde{\phi}(\tau) = 2\int_0^\infty \mathrm{d}\omega \frac{J(\omega)}{\omega^2}(1 - F(\omega, d))\frac{\cos(\omega\tau)}{\sinh(\beta\omega/2)}. \quad \text{(A5)}$$

Using a super-Ohmic form of spectral density, $J(\omega) = \alpha\omega^3\omega_0^{-2}\mathrm{e}^{-\omega/\omega_c}$, and assuming system-bath coupling in three dimensions such that $F(\omega, d) = \mathrm{sinc}(\omega d/c)$, allows $\tilde{\phi}(\tau)$ to be found analytically. We find $\tilde{\phi}(\tau) = \phi_0 C(x, y, \tau')$, where

$$\begin{aligned} C(x,y,\tau') = \frac{-i}{2\pi x}\Big[&\psi\left(\frac{1}{2}+\frac{1}{y}-\frac{i}{\pi}(\tau'+x)\right) \\ &-\psi\left(\frac{1}{2}+\frac{1}{y}-\frac{i}{\pi}(\tau'-x)\right) \\ &+\psi\left(\frac{1}{2}+\frac{1}{y}+\frac{i}{\pi}(\tau'-x)\right) \\ &-\psi\left(\frac{1}{2}+\frac{1}{y}+\frac{i}{\pi}(\tau'+x)\right)\Big] \\ +\frac{1}{\pi^2}\Big[&\psi'\left(\frac{1}{2}+\frac{1}{y}-\frac{i}{\pi}\tau'\right) \\ &-\psi'\left(\frac{1}{2}+\frac{1}{y}+\frac{i}{\pi}\tau'\right)\Big]. \end{aligned}$$

Here, $\phi_0 = 2\pi^2\alpha/(\omega_0^2\beta^2)$, $x = \pi d/c\beta$, $y = \omega_c\beta$, $\tau' = \pi\tau/\beta$, $\psi(z)$ is the the digamma function, and $\psi'(z)$ its first derivative.

To proceed, we assume a high-temperature or strong-coupling regime, such that the dominant contributions to the integrals in Eqs. (A3) and (A4) will come from the peak in $\tilde{\phi}(\tau)$ at $\tau = 0$. More specifically, inspection of $C(x, y, \tau')$ reveals that for $y \gg 1$ (the scaling limit of large $\omega_c$), we require $\phi_0 \gg 1$ for large $x$ (weak correlations), or $\phi_0 x^2 \gg 1$ for small $x$ (strong correlations), in order for an expansion of $\tilde{\phi}(\tau)$ around $\tau = 0$ to be valid. These definitions of the high-temperature (or strong-coupling) regime tally with the expansion parameters identified in Ref. 11. In the opposite limit, $y \ll 1$, we generally need $\phi_0 x^2 y^3/\pi^4 \gg 1$, except in the limit of very large separations (vanishing correlations), $x \to \infty$, where $\phi_0 y \gg 1$ is the relevant condition.

With these conditions in mind, we therefore expand $\tilde{\phi}(\tau)$ to second order in $\tau' = \pi\tau/\beta$, which gives

$$\tilde{\phi}(\tau) \approx \phi_0(C_0(x, y) - \tau'^2 C_2(x, y)), \quad \text{(A6)}$$

where

$$\begin{aligned} C_0(x,y) =& \frac{i}{\pi x}\Big[\psi\Big(\frac{1}{2}+\frac{1}{y}+\frac{ix}{\pi}\Big) - \psi\Big(\frac{1}{2}+\frac{1}{y}-\frac{ix}{\pi}\Big)\Big] \\ &+ \frac{2}{\pi^2}\psi'\Big(\frac{1}{2}+\frac{1}{y}\Big), \end{aligned} \quad \text{(A7)}$$

and

$$\begin{aligned} C_2(x,y) =& \frac{i}{2\pi^3 x}\Big[\psi''\Big(\frac{1}{2}+\frac{1}{y}+\frac{ix}{\pi}\Big) - \psi''\Big(\frac{1}{2}+\frac{1}{y}-\frac{ix}{\pi}\Big)\Big] \\ &+ \frac{1}{\pi^4}\psi'''\Big(\frac{1}{2}+\frac{1}{y}\Big). \end{aligned} \quad \text{(A8)}$$

Additionally, contributions to Eqs. (A3) and (A4) from terms containing a factor of $\exp[-\tilde{\phi}(\tau)]$ will vanish, since

they tend to zero in the high-temperature limit, allowing us to write

$$\gamma_{ul}(\eta) \approx \frac{B^2 \mathrm{e}^{\beta\eta/2}\beta}{2\pi}\mathrm{e}^{\phi_0 C_0}\int_{-\infty}^{+\infty} d\tau' \mathrm{e}^{i\tau'\eta\beta/\pi}(\mathrm{e}^{-\tau'^2\phi_0 C_2}-1). \tag{A9}$$

We note that the second term in the integrand does not contribute since the saddle point integration does not necessarily require that the integration limits be infinite. The remaining integral is Gaussian and we arrive at the result

$$\gamma_{ul}(\eta) = \frac{\beta B^2 \mathrm{e}^{\phi_0 C_0(x,y)}}{2\sqrt{\pi C_2(x,y)\phi_0}}\mathrm{e}^{\beta\eta/2}\mathrm{e}^{-\beta^2\eta^2/(4\pi^2 C_2(x,y)\phi_0)}, \tag{A10}$$

which reduces to

$$\gamma_{ul}(\eta) \approx \gamma_{ul}(0) = \frac{\beta B^2 \mathrm{e}^{\phi_0 C_0(x,y)}}{2\sqrt{\pi C_2(x,y)\phi_0}}, \tag{A11}$$

if the temperature is high enough such that $1/\eta\beta \gg 1$.

It remains now to determine the bath renormalisation factor $B$, given by Eq. (8). To do so it is helpful to separate vacuum and thermal contributions. We write $B = B_0 B_{\mathrm{th}}$, where

$$B_0 = \exp\left[-\int_0^\infty d\omega \frac{J(\omega)}{\omega^2}(1-F_D(\omega,d))\right], \tag{A12}$$

and

$$B_{\mathrm{th}} = \exp\left[-\int_0^\infty d\omega \frac{J(\omega)}{\omega^2}(1-F_D(\omega,d))(\coth(\beta\omega/2)-1)\right]. \tag{A13}$$

Inserting the spectral density, and again assuming system-bath coupling in three dimensions, we find

$$B_0 = \exp\left[-\alpha\frac{\omega_c^2}{\omega_0^2}\left(\frac{(d\omega_c/c)^2}{1+(d\omega_c/c)^2}\right)\right], \tag{A14}$$

and

$$B_{\mathrm{th}} = \exp\left[\frac{\phi_0}{2\pi^2}\left(\frac{i\pi}{x}\big(H(y^{-1}-ix/\pi)-H(y^{-1}+ix/\pi)\big) - 2\psi'(1+y^{-1})\right)\right], \tag{A15}$$

where $H(m) = \sum_{i=1}^m (1/i)$ is the $m$th harmonic number. We note that in the infinite separation (uncorrelated) limit, one finds $B_0(d\to\infty) = \exp[-\alpha(\omega_c^2/\omega_0^2)]$, and

$$B_{\mathrm{th}} = \exp[\alpha(\omega_c^2/\omega_0^2)(1-y^{-2}(\zeta(2,1+y^{-1})+\zeta(2,y^{-1})))], \tag{A16}$$

where $\zeta(s,a)$ is the generalised Riemann zeta function.


* Electronic address: dara.mccutcheon@ucl.ac.uk
† Electronic address: ahsan.nazir@ucl.ac.uk



[1] H. Lee, Y.-C. Cheng, and G. R. Fleming, Science **316**, 1462 (2007).
[2] G. S. Engel, T. R. Calhoun, E. L. Read, T.-K. Ahn, T. Mancal, Y.-C. Cheng, R. E. Blankenship, and G. R. Fleming, Nature **446**, 782 (2007).
[3] T. R. Calhoun, N. S. Ginsberg, G. S. Schlau-Cohen, Y.-C. Cheng, M. Ballottari, R. Bassi, and G. R. Fleming, J. Phys. Chem. B **113**, 16291 (2009).
[4] E. Collini and G. D. Scholes, Science **323**, 369 (2009).
[5] E. Collini and G. D. Scholes, J. Phys. Chem. A **113**, 4223 (2009).
[6] E. Collini, C. Y. Wong, K. E. Wilk, P. M. G. Curmi, P. Brumer, and G. D. Scholes, Nature **463**, 644 (2010).
[7] G. Panitchayangkoon, D. Hayes, K. A. Fransted, J. R. Caram, E. Harel, J. Wen, R. E. Blankenship, and G. S. Engel, Proc. Natl. Acad. Sci. **107**, 12766 (2010).
[8] I. P. Mercer, Y. C. El-Taha, N. Kajumba, J. P. Marangos, J. W. G. Tisch, M. Gabrielsen, R. J. Cogdell, E. Springate, and E. Turcu, Phys. Rev. Lett. **102**, 057402 (2009).
[9] J. M. Womick, S. A. Miller, and A. M. Moran, J. Phys. Chem. B **113**, 6630 (2009).
[10] J. Gilmore and R. H. McKenzie, J. Phys.: Condens. Matter **17**, 1735 (2005).
[11] A. Nazir, Phys. Rev. Lett. **103**, 146404 (2009).
[12] S. Jang, Y.-C. Cheng, D. R. Reichman, and J. D. Eaves, J. Chem. Phys. **129**, 101104 (2008).
[13] S. Jang, J. Chem. Phys. **131**, 164101 (2009).
[14] J. Prior, A. W. Chin, S. F. Huelga, and M. B. Plenio, Phys. Rev. Lett. **105**, 050404 (2010).
[15] M. Thorwart, J. Eckel, J. H. Reina, P. Nalbach, and S. Weiss, J. Phys. Chem. Lett. **478**, 234 (2009).
[16] A. Ishizaki and G. R. Fleming, J. Chem. Phys. **130**, 234111 (2009).
[17] A. Kimura and T. Kakitani, J. Phys. Chem. A **111**, 12042 (2007).
[18] J. Roden, A. Eisfeld, W. Wolff, and W. T. Strunz, Phys. Rev. Lett. **103**, 058301 (2009).
[19] H. Hossein-Nejad and G. D. Scholes, New J. Phys. **12**, 065045 (2010).
[20] D. L. Andrews, Chem. Phys. **135**, 195 (1989).
[21] T. Förster, Discuss. Faraday Soc.. **27**, 7 (1959).
[22] D. I. Dexter, J. Chem. Phys. **21**, 836 (1952).
[23] G. D. Scholes, Annu. Rev. Phys. Chem. **54**, 57 (2003).
[24] D. Beljonne, C. Curutchet, G. D. Scholes, and R. J. Silbey, J. Phys. Chem. B. **113**, 6583 (2009).
[25] H.-P. Breuer and F. Petruccione, *The Theory of Open Quantum Systems* (Oxford University Press, 2002).
[26] A. Olaya-Castro, C. F. Lee, F. F. Olsen, and N. F. Johnson, Phys. Rev. B **78**, 085115 (2008).
[27] M. Mohseni, P. Rebentrost, S. Lloyd, and A. Aspuru-Guzik, J. Chem Phys. **129**, 174106 (2008).
[28] M. B. Plenio and S. F. Huelga, New J. Phys. **10**, 113019 (2008).
[29] F. Caruso, A. W. Chin, A. Datta, S. F. Huelga, and M. B. Plenio, J. Chem. Phys. **131**, 105106 (2009).
[30] P. Rebentrost, M. Mohseni, I. Kassal, S. Lloyd, and A. Aspuru-Guzik, New. J. Phys. **11**, 033003 (2009).
[31] P. Rebentrost, M. Mohseni, and A. Aspuru-Guzik, J. Phys.

Chem. B **113**, 9942 (2009).
[32] A. W. Chin, A. Datta, F. Caruso, S. F. Huelga, and M. B. Plenio, New J. Phys. **12**, 065002 (2010).
[33] F. Fassioli, A. Nazir, and A. Olaya-Castro, J. Phys. Chem. Lett. **1**, 2139 (2010).
[34] P. Rebentrost, R. Chakraborty, and A. Aspuru-Guzik, J. Chem. Phys. **131**, 184102 (2009).
[35] T. Renger and R. A. Marcus, J. Chem. Phys. **116**, 9997 (2002).
[36] S. Rackovsky and R. Silbey, Mol. Phys. **25**, 61 (1973).
[37] J. A. Legwater, J. Chem. Phys. **100**, 14403 (1996).
[38] J. B. Gilmore and R. H. McKenzie, Chem. Phys. Lett. **421**, 266 (2006).
[39] Y.-C. Cheng and G. R. Fleming, Annu. Rev. Phys. Chem. **60**, 241 (2009).
[40] A. Olaya-Castro and G. D. Scholes, to appear in Int. Rev. Phys. Chem.
[41] T. F. Soules and C. B. Duke, Phys. Rev. B. **3**, 262 (1971).
[42] V. M. Kenkre and R. S. Knox, Phys. Rev. B **9**, 5279 (1974).
[43] I. I. Abram and R. Silbey, J. Chem. Phys. **63**, 2317 (1975).
[44] W. M. Zhang, T. Meier, V. Chernyak, and S. Mukamel, J. Chem. Phys. **108**, 7763 (1998).
[45] M. Yang and G. R. Fleming, Chem. Phys. **282**, 163 (2002).
[46] V. I. Novoderezhkin, M. A. Palacios, H. van Amerongen, and R. van Grondelle, J. Phys. Chem. B **108**, 10363 (2004).
[47] T. Renger and R. A. Marcus, J. Phys. Chem. A **107**, 8404 (2003).
[48] H. Sumi, J. Phys. Chem. B **103**, 252 (1999).
[49] G. D. Scholes and G. R. Fleming, J. Phys. Chem. B **104**, 1854 (2000).
[50] S. Jang, M. D. Newton, and R. J. Silbey, Phys. Rev. Lett. **92**, 218301 (2004).
[51] A. Wurger, Phys. Rev. B. **57**, 347 (1998).
[52] M. Tanaka and Y. Tanimura, J. Chem. Phys. **132**, 214502 (2010).
[53] P. Nalbach, J. Eckel, and M. Thorwart, New J. Phys. **12**, 065043 (2010).
[54] S. Tornow, R. Bulla, F. B. Anders, and A. Nitzan, Phys. Rev. B. **78**, 035434 (2008).
[55] I. Wilson-Rae and A. Imamoglu, Phys. Rev. B **65**, 235311 (2002).
[56] E. Hennebicq, D. Beljonne, C. Curutchet, G. D. Scholes, and R. J. Silbey, J. Chem. Phys. **130**, 214505 (2009).
[57] Z. G. Yu, M. A. Berding, and H. Wang, Phys. Rev. E **78**, 050902(R) (2008).
[58] X. Chen and R. J. Silbey, J. Chem. Phys. **132**, 204503 (2010).
[59] B. A. West, J. M. Womick, L. E. McNeil, K. J. Tan, and A. M. Moran, J. Phys. Chem. C. **114**, 10580 (2010).
[60] M. Sarovar, Y.-C. Cheng, and K. B. Whaley, arXiv:0911.5427.
[61] A. Ishizaki and G. R. Fleming, J. Chem. Phys. **130**, 234110 (2009).
[62] R. Silbey and R. A. Harris, J. Chem. Phys. **80**, 2615 (1984).
[63] D. P. S. McCutcheon, A. Nazir, S. Bose, and A. J. Fisher, Phys. Rev. A. **80**, 022337 (2009).
[64] D. A. Lidar, I. L. Chuang, and K. B. Whaley, Phys. Rev. Lett. **81**, 2594 (1998).
[65] P. Zanardi and M. Rasetti, Phys. Rev. Lett. **79**, 3306 (1997).
[66] U. Weiss, *Quantum Dissipative Systems (3rd Ed.)* (World Scientific, 2008).
[67] A. J. Ramsay, A. V. Gopal, E. M. Gauger, A. Nazir, B. W. Lovett, A. M. Fox, and M. S. Skolnick, Phys. Rev. Lett. **104**, 017402 (2010).
[68] E. Rozbicki and P. Machnikowski, Phys. Rev. Lett. **100**, 027401 (2009).
[69] A. J. Leggett, S. Chakravarty, A. T. Dorsey, M. Fisher, A. Garg, and W. Zwerger, Rev. Mod. Phys. **59**, 1 (1987).
[70] B. D. Gerardot, S. Strauf, M. J. A. de Dood, A. M. Bychkov, A. Badolato, K. Hennessy, E. L. Hu, D. Bouwmeester, and P. M. Petroff, Phys. Rev. Lett **95**, 137403 (2005).
[71] A. O. Govorov, Phys. Rev. B **71**, 155323 (2005).
[72] A. Kolli et al., in preparation.
[73] N. Makri, J. Phys. Chem. A **102**, 4414 (1998).
[74] To ensure this we keep $V < \omega_c$, where $\omega_c$ is a high-frequency cut-off in the bath spectral density (see Eq. (32)).
[75] Although we would usually expect $V$ to change with varying separation $d$, we keep it fixed for all plots presented here in order to isolate the role played by the environmental correlations.